Journal of Ceramic Processing Research. Vol. 23, No. 5, pp. 725~736 (2022)
(Received 17 May 2022, Received in revised form 14 June 2022, Accepted 18 June 2022)
https://doi.org/10.36410/jcpr.2022.23.5.725

J O U R N A L O F
Ceramic Processing Research

Boron nitride nanostructures reinforced nanohydroxyapatite: bifunctional nanocomposite for potential orthopedical use and ciprofloxacin controlled delivery

Luísa Arantes Fernandes Vieira, Isabela Barreto da Costa Januário Meireles and Edésia Martins Barros Sousa
Comissão Nacional de Energia Nuclear – Centro de Desenvolvimento da Tecnologia nuclear – (CNEN/CDTN), Laboratório de Materiais Nanoestruturados para Bioaplicações, Av. Presidente Antônio Carlos 6.627, Pampulha, 31270-901, Belo Horizonte, MG, Brazil

One of the most promising options for bone defects or lesions is the use of synthetic materials as bone substitutes. Thus, the objective of the present work was to synthesize a nanocomposite of HA and BNNS, as a reinforcement phase, to obtain a material with satisfactory mechanical properties as well as bifunctional, with the incorporation of ciprofloxacin to evaluate the potential of the system as a drug delivery. The nanocomposites obtained were characterized by X-ray diffraction (XRD), Fourier transform infrared spectroscopy (FTIR), thermogravimetry (TG), nitrogen adsorption by BET and BJH methods, scanning electron microscopy (SEM) and electron microscopy transmission (TEM). The Vickers hardness test and nanoindentation showed an increase in the mechanical strength of the nanocomposites with the insertion of the reinforcement phase, thus corroborating the promising character of BNNS as a reinforcement agent for HA. A biocompatibility assay was performed to assess the potential of the samples as effective biomaterials. The nanocomposites showed high cell viability indicating that the system does not present cytotoxicity. Drug loading and in vitro release show that the system can provide rapid drug delivery, giving antibacterial effects at the infected site, indicating that the nanocomposite, a bioceramic, is suitable for the application.

Keywords: Hydroxyapatite, Boron nitride nanosheets, Reinforcement, Bone repair.

Introduction

The deterioration of the human body, due to the increase in life expectancy, has become an undesirable issue since it has not been possible to slow down its aging process. One of the natural consequences of aging is a decrease in bone strength, an increase in the probability of fracture, and diseases that generate different bone defects. Bone diseases account for half of the chronic diseases in people over 50 years of age. Large defects or injuries, whether caused by old age or by accidents, unhealed fractures, or tumor resection are serious problems in orthopedics and harm the individual's health and quality of life [1].

Hydroxyapatite, a calcium phosphate, stand out in making bone substitutes due to its similarity to the inorganic phase of bones [2]. HA constitutes a large part of human hard tissue, representing approximately 60% of natural bone mass [3] in addition to different proportions of dental tissue. It is often used as a bone and dental substitute due to its bioactivity, biocompatibility, and its osteoinductive propriety [4], assisting in the adhesion and proliferation of osteoblasts [5].

Despite having interesting characteristics for orthopedic application, HA has inferior mechanical properties when compared to human bones. Due to its low resistance to fracture, its use in the orthopedic area is limited to regions not susceptible to great efforts. To expand its use as a bone substitute, its mechanical properties can be improved by controlling its density, microstructure, and insertion of reinforcement phases. Ramesh et al. studied the influence of two-step sintering on the mechanical properties of HA and noted that the sintering model plays a role in the densification of HA, resulting in an improvement in its hardness and fracture resistance [6]. Nazarpak et al., studied the influence of sintering on the mechanical properties and microstructure of HA, and concluded that high sintering temperatures improve the microstructure of the material, which leads to an increase in its mechanical strength [7]. Several methods of microstructural reinforcement of HA have been studied, mainly through the formation of composites [8-14]. Ferreira et al., investigated the influence of the percentage of zirconia on the mechanical properties and densification of zirconia/HA composites. They concluded that 85/15 and 80/20 Zr/HA samples showed better mechanical behavior in their composition as the increased trabecular bone mineral density and the

*Corresponding author:
Tel : +55-31-3439-9523
E-mail: sousaem@cdtn.br

connection between the scaffold and bone tissue [15]. Al-allaq et al., introduced carbon nanotubes and high-density polyethylene in the hydroxyapatite matrix to form an orthopedic biocomposite. The composite showed improvement in the tensile and microhardness tests with the addition of the reinforcement phase [16].

Boron nitride (BN) is a binary chemical compound formed only by atoms of boron and nitrogen [17]. The advancement of nanoscience and nanotechnology led to the discovery of several BN structures, such as boron nitride nanosheets (BNNSs), boron nitride nanotubes (BNNTs), and boron nitride nanoribbons (BNNRs). All these nanostructures are based on the hexagonal phase of BN [18].

As two-dimensional layered nanomaterials, hexagonal boron nitride nanosheets (BNNSs) have raised great research interest due to their distinct properties and thus become promising materials to boost the mechanical, thermal, electrical, and optical properties of ceramics nanocomposites [19].

BN nanosheets have exceptional mechanical properties with great fracture strength (165 GPa) and high Young's modulus (0.8 TPa) [20]. They also present a non-toxic character, characteristics that make them a promising agent for biological applications. Experiments have demonstrated that BNNSs are non-cytotoxic, suggesting that they can be widely used as biocompatible materials for biomedical, therapeutic, and diagnostic applications [21].

Some works are reported in the literature using several h-BN nanostructures as ceramics reinforcement phase and the results are most satisfactory. Shuai et al. used BN nanostructures as a method of strengthening β-TCP scaffolds. The addition of 4% of BNNT generated a 46% increase in elastic modulus, 39% in material hardness, and 35% in fracture strength [22]. Another study relates h-BN and HA, to improve the mechanical properties of HA adding BN nanoplates to the matrix in different mass variations. The work concluded that the addition above 1% by mass of BN is not beneficial to the system, with the pure HA phase being mechanically more resistant [23].

Wang et al. synthesized a composite of HA and h-BN for potential application as a scaffold. The maximum flexural strength and elastic modulus were observed at 0.25 and 0.13 wt% BN addition, respectively. Despite that, there was a decrease in the hardness of the material with the addition of the reinforcement phase. Furthermore, from the results of biological tests in vitro, BN/HA composites showed no adverse effects [24].

These studies were particularly relevant to open future works with this innovative system since it seems to be a promisor to be used as a biomedical device. However, it is noted that none of these studies explored the potential of the material as drug delivery, also acting in the prophylaxis of possible infections caused by surgery for implementing the material.

Therefore, it is expected that by incorporating BNNSs into the HA matrix, the fracture strength can be improved, making it less brittle and allowing it to be used in a wide range of applications. In this context, this study was motivated by the promising potential of this system for orthopedical applications and, concomitantly, it sought to evaluate the system as a bifunctional bioceramic material through ciprofloxacin incorporation and in vitro release test, making this innovative research.

Experimental

Materials

Pluronic F-127 (F-127), calcium nitrate tetrahydrate ($Ca(NO_3)_2 \cdot 4H_2O$), potassium phosphate dibasic trihydrate ($K_2HPO_4 \cdot 3H_2O$), ammonium hydroxide (NH_4OH), boron (B), iron (III) oxide (Fe_2O_3), magnesium oxide (MgO), sulfuric acid (H_2SO_4), and nitric acid (HNO_3) were purchased from Sigma-Aldrich. Water solutions were prepared with purified water obtained from Milli-Q® Direct Water Purification System (Millipore—Burlington, EUA).

Methods

Synthesis of HA

Nano hydroxyapatite was synthesized from the preparation of two precursor solutions. Solution (i) was prepared with the complete dissolution of 0.8 g of F-127, as a template agent, in 40 mL of Milli-Q® water and the subsequent addition of calcium nitrate to obtain a concentration of 0.167 M. Solution (ii) was prepared by dissolving dipotassium phosphate to obtain a concentration of 0.1 M. Both solutions were adjusted to pH 10 with the addition of 3 M ammonium hydroxide. Solution (i) was stirred and then the solution (ii) was slowly dropped onto solution (i). The suspension was kept under stirring at room temperature and, after this process, a thermal treatment was carried out at 150 °C in a hydrothermal reactor for 3 hours. Then, the suspension was centrifuged, and vacuum filtrated with Milli-Q® water and ethanol washing. The filtered material was kept in an oven for 24 hours at a temperature of 60 °C to dry, and then it was calcined for 6 hours at 600 °C to promote the complete removal of the surfactant, obtaining, in the end, a fine white powder.

Synthesis of BNNS

The synthesis of BNNS was performed using the CVD technique in a tubular oven. Boron, iron oxide (III) and magnesium oxide were mixed in a 1:1:1 ratio and macerated for complete homogenization. They were also sieved and distributed equally in an alumina recipient which was inserted inside a stainless-steel tube with one end closed. The synthesis was carried out

under an atmosphere of nitrogen and ammonia. During heating, N_2 flow was maintained in an inert atmosphere. When it reached 1300 ºC, the nitrogen flow was interrupted and the NH_3 was inserted, remaining constant for 2 hours. Then, cooling was started, again in an inert nitrogen atmosphere. The purification and hydroxylation of BNNSs occurred in an acidic medium containing sulfuric acid and nitric acid in a 3:1 ratio. The suspension was kept under stirring at 80 °C for 3 hours. Then, the solution is vacuum filtered with Milli-Q® water washing and dried for 24 hours in an oven at 60 ºC.

Synthesis of nanocomposites

For the synthesis of the bioceramic nanocomposites, HA-BNNS, the same methodology used during the HA synthesis was followed, with one modification in the composition of the solution (i) by adding hydroxylated BNNS dispersed in Milli-Q® water. After the hydrothermal treatment, the material was washed, dried, and calcined following the same HA synthesis protocol. The samples were named HA, HA-3BN, and HA-10BN for 0%, 3%, and 10% BNNS contents, respectively.

Characterization of materials

The X-ray diffraction (XRD, Rigaku) analysis with Cu-Kα radiation was conducted to characterize the phase constituents of all samples before and after sintering to identify possible new phases resulting from heat treatment. The 2-theta varies from 10 º to 80 º with a step size of 0.02 º and a scanning rate of 2 º min^{-1}. Chemical bonds and functional groups of the nanocomposites were detected using a Fourier transform infrared spectroscopy (FT-IR, Thermo Nicolet 6700). The absorbance was in the range of 4000 and 400 cm^{-1}. The morphology of surface was observed by field emission scanning electron microscopy (Quanta 3D FEG, FEI) and transmission electron microscopy (Tecnai G2-12-FEI). The specific surface area and pore size distribution (Autosorb-iQ, Quantachrome) were determined by N_2 adsorption using the BET and BJH methods, respectively.

Mechanical tests

To obtain specimens for the mechanical tests, the samples, in powder form, were pressed, through a hydraulic press (Ciola), with a load of 6 t cm^{-2} in a time of 5 seconds. Each specimen had 11.5 mm in diameter and approximately 3 mm in thickness. They were sintered under an inert atmosphere, at a temperature of 900 ºC for 1 hour in a sintering furnace (Barnstead Thermolyne International). Nanoindentation test was performed using an ultra-micro hardness tester (DUH 211, Shimadzu) with a constant loading/unloading rate for 10 s and 3 s hold at the peak load of 30 mN. Elastic modulus (E) had been calculated from the load-displacement curves using the Oliver-Pharr method (OLIVER; PHARR, 1992). To determine the hardness of the samples, Vickers microhardness of the polished specimens was measured using a microindentation device (Wolpert Wilson Instruments). The specimens were subjected to a load of 1 kg in a waiting time of 10 s. Each specimen was marked with 5 points in different areas to obtain an average value. The fracture toughness was calculated using the indentation and crack patterns, visualized through SEM, by the following equation [25]:

$$K_{IC} = 0.016(E/H_V)^2 P/c^{1,5}$$

where H_V is the Vickers microhardness (GPa), E is the elastic modulus (GPa), P is the indentation load (N), c is the crack length (m).

Drug loading and in vitro release

To evaluate a potential application of the HA/BN system as drug delivery, controlled release trials were performed using the drug ciprofloxacin. Ciprofloxacin is a drug with a large spectrum of action and can be used in the treatment of bone infections. The adsorption of ciprofloxacin within HA and HA/BNNSs nanocomposites was performed by soaking 100 mg of the powder sample in a drug solution (1 mg/mL) with a 1:1 rate and kept under magnetic stirring for 72 h. The ciprofloxacin solution was subjected to pH variation to obtain complete solubilization of the drug. The mixture was filtered and dried for 24 h at 60 °C. Elemental analysis (EA 2400 Series II CHNS/O-PerkinElmer) and thermogravimetry analysis (DTG-60H TGA-Shimadzu) were performed in all samples to evaluate the percentage of ciprofloxacin incorporated.

For release assays, HA and HA/BNNSs nanocomposites samples were immersed in simulated body fluid (SBF). This suspension was put into a dialysis tube (cutoff Mn = 3500) and then placed in a flask with 40 mL of SBF under constant stirring at a rate of 50 rpm. The UV spectrometry procedure (UV-VIS V-2401-Shimadzu) was used to monitor the amount of loaded and released ciprofloxacin as a function of time. The concentration of ciprofloxacin in SBF was determined by the intensity of the absorption band at 277 nm.

Biocompatibility studies

The nanocomposites biocompatibility was investigated by MTT assay. MRC-5 cells were seeded (5.0×10^3 cells/well) on 96 well plates. After 24 h incubation (37 °C, 95% humidity, and 5% CO_2), cells were treated with the materials in four concentrations (10, 50, 100, and 200 μg mL^{-1}). Experiments were performed in triplicate with 3 blank and 3 control wells. After another 48 h of incubation, the media of the wells were removed and washed with phosphate-buffered saline (PBS). Next, 10 μL of MTT solution (5 mg mL^{-1}) and 90 μL of DMEM were added per well. The plates were incubated for 2 h until the formazan crystallization.

Then, MTT+DMEM solution was removed from each well and 50 µL of DMSO and 25 µL of DMEM were added to dissolve the formazan crystals. The absorbance was measured at 570 nm using a Multiskan GO microplate reader (Thermo Scientific, USA). The absorbance from blank wells was subtracted from each measurement and the cell viability was calculated as a function of the control group absorbance.

Results and Discussion

XRD

Fig. 1(a) shows the diffractograms of the HA and nanocomposites. All samples are aligned with file 09-0432 from the ICDD PDF database. It is then possible to estimate the formation of HA, with the hexagonal arrangement, space group P63/m, and characteristic peaks at Bragg angle 2θ of approximately 31.7 º, 32 º, 33 º, and 34 º. These peaks can be attributed to reflections from the planes (211), (112), (300), and (202) respectively, as shown in the image. It is possible to observe in HA-10BN nanocomposite the presence of a small peak at the Bragg angle 2θ of approximately 27 º corresponding to the peak (002) of the h-BN reinforcement phase coming from the BNNS, as seen in Fig. 1-b. This peak is not as apparent in the HA-3BN sample, which can be attributed to the small concentration of the phase in the nanocomposite. This result suggests obtaining a crystalline material with HA as the majority phase, both in pure samples and in composites, as expected.

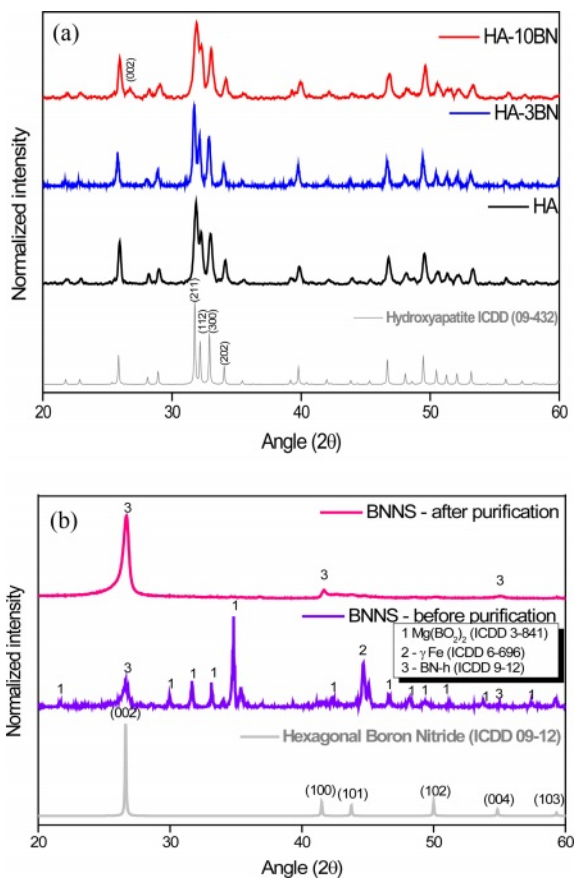

Fig. 1. XRD of (a) HA and nanocomposites and (b) BNNS before and after purification.

Fig. 1(b) shows the diffractogram of BNNS samples. It is possible to identify the presence of h-BN, Mg $(BO_2)_2$, and *y*Fe phases in the sample before purification. The impurities came from the reagents used in the synthesis and were removed in the purification step since the diffraction pattern of the BNNS after the purification only indicates peaks related to h-BN. Typical peaks of the hexagonal phase of boron nitride at 2θ = 26.8 °; 41.6 ° and 55.0 ° are present. Such peaks can be identified at reflections from the planes (002), (100), and (004), respectively.

FTIR

Fig. 2 shows the results of the FTIR analysis of the BNNS and nanocomposites samples. In the BNNS spectra, the presence of two bands related to BN is noted. The asymmetric band centered at 1380 cm^{-1} corresponds to the stretching of the B-N bond and the band at 790 cm^{-1} is attributed to the B-N-B bond [26].

The spectra of HA, and its nanocomposites present transmittance bands referring to the characteristic vibrational modes of HA [27]. The bands at 470 cm^{-1}, 570 cm^{-1}, 602 cm^{-1}, 960 cm^{-1} and 1030 cm^{-1} correspond to the phosphate vibrational modes. The band refers to the stretching of the OH^- that can be observed at 630 cm^{-1} [28, 29]. The great difference between HA and nanocomposites is the presence of the bands coming from the BNNS, thus indicating its presence in the nanocomposite. This result corroborates the information obtained through the X-ray diffraction analysis and indicates the formation of the HA/BNNS nanocomposite.

In addition to the characteristic bands of HA and BNNS, evidence of the presence of boron oxide is present in the nanocomposites spectra. Bands at a wavelength of approximately 1260 cm^{-1}, 1244 cm^{-1}, and 1211 cm^{-1} are related to the elongation vibrations of B-O-H, which can be seen in region A of the spectra. The bands at the lengths of 770 cm^{-1}, and 740 cm^{-1} are related to the vibrations of the B-O bond [30] and are highlighted in region B. Such bands appear in HA-3BN and HA-10BN nanocomposites.

It is known that sintering is an important step for material densification and, consequently, improves its mechanical properties. However, the sintering of hydroxyapatite can cause the absence of OH radicals through heating. At temperatures close to 850-900 ºC HA dehydroxylates and at temperatures above that, it decomposes into other calcium phosphates [31]. No evidence of the formation of new calcium phosphate phases was found, but the appearance of boron oxides may be an indication that there was dehydroxylation of HA. In fact, analyzing the spectrum in the region

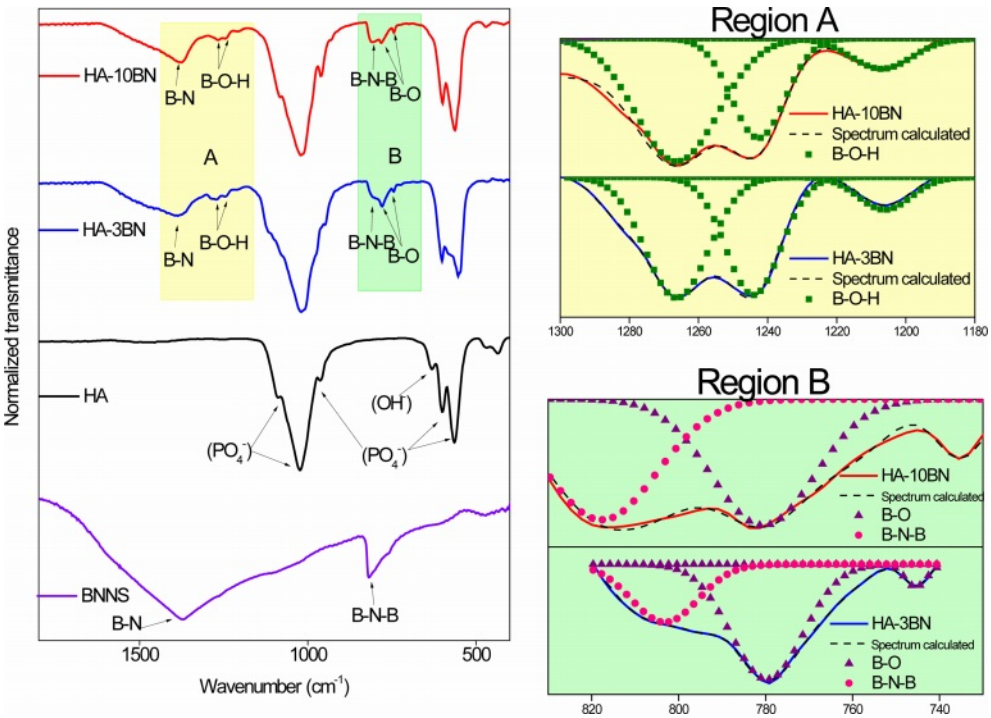

Fig. 2. FTIR of HA and HA-BN nanocomposites.

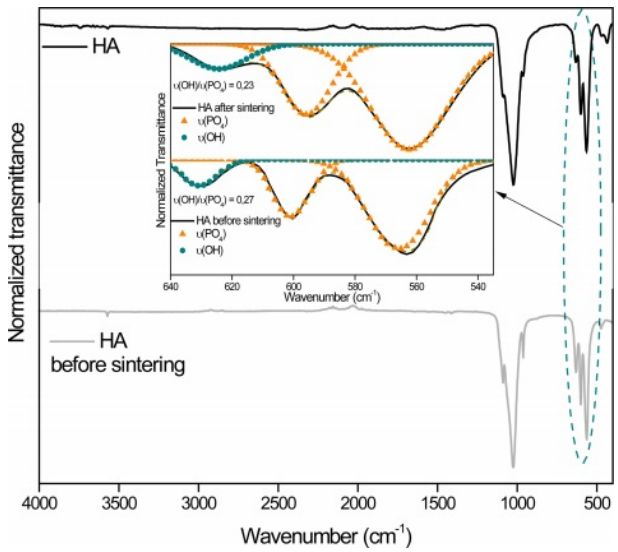

Fig. 3. Normalized spectra of HA before and after sintering.

between 650 cm^{-1} and 535 cm^{-1} (Fig. 3), a decrease in the intensity of the OH^- band is observed in the HA sample. When normalizing the intensities, this fact becomes evident, since the relative intensity of OH^- before sintering is 0.27 and after sintering it drops to 0.23. In nanocomposites, the same band disappeared after sintering, as can be seen in Fig. 4.

It is suggested that there was a binding process between oxygen, from the dehydroxylation of HA during the sintering, with boron. The boron in question can be a remnant of the amorphous reagent, coming from the synthesis. Works by the LMNB-CDTN research group [32-34] point to the presence of amorphous boron as a non-material reacted during the synthesis, which can lead to the appearance of other phases.

Wang et al. noticed the same behavior when sintering the HA-BN composites, indicating the presence of hydrated boron oxide in samples. This result did not change the biological properties of the material since they did not show cytotoxicity even with this undesired presence. However, the authors related the existence of boron oxide to the formation of micropores in the composite. In contrast, the same sintering product is responsible for eliminating the nanopores present in the material and densifying the walls of the micropores. As a result, the number of nanopores on the polished surface and fracture surface of BN/HA composites was decreased with the increase in BN content, which increased the fracture strength of the material [24].

N_2 adsorption

Nitrogen adsorption and desorption isotherms of the samples are shown in Fig. 5. Through the result of the test, applying the equations of BET and BJH, the values of surface area (S_{BET}), volume (V_P), and pore diameter (D_P) are shown in Table 1.

All the isotherms can be classified as type IV with type-H3 hysteresis loop which is often observed with aggregates of plate-like particles that give rise to slit-shape pores [35]. Furthermore, this result indicates that the BNNS addition did not lead to significant changes in the pore structure of nanoparticles.

A decrease in S_{BET}, V_P, and D_P occurs when BNNS is

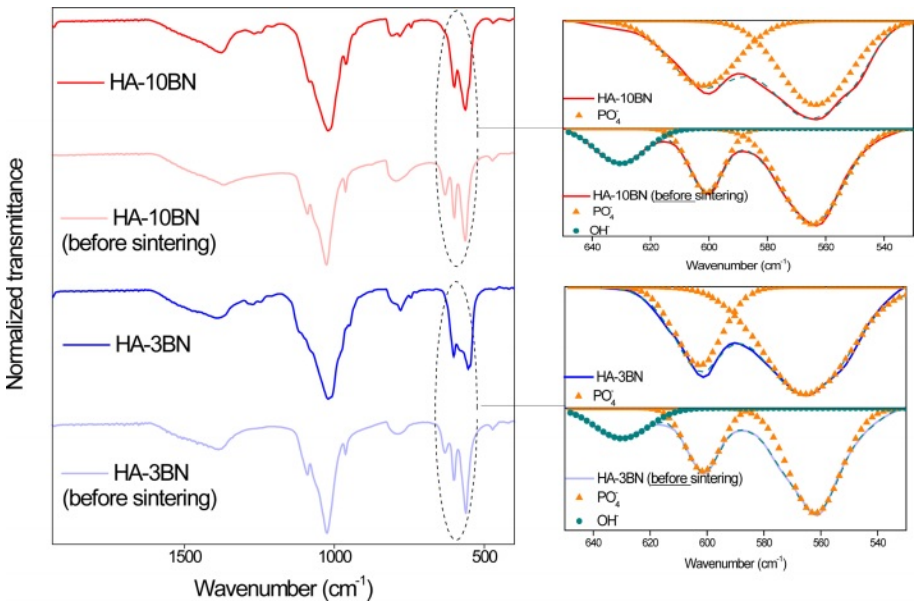

Fig. 4. Normalized spectra of nanocomposites before and after sintering.

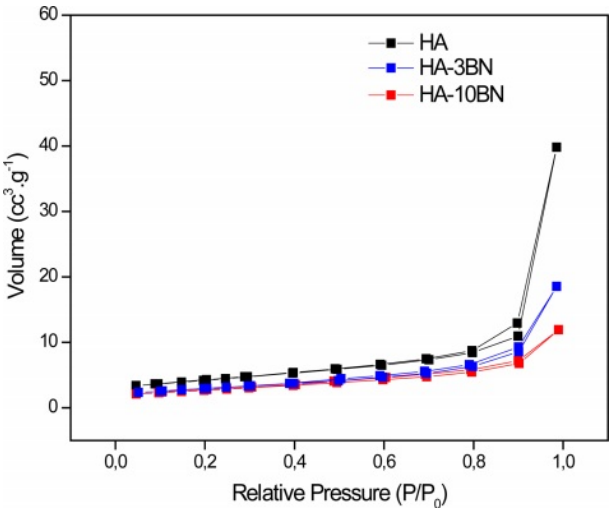

Fig. 5. The type III N_2 adsorption-desorption isotherms for the nanocomposite samples.

Table 1. Textural and porosity parameters obtained through BET and BJH methods applied on the N_2 adsorption-desorption isotherms data.

Samples	S_{BET} ($m^2 \cdot g^{-1}$)	V_P ($cc^3 \cdot g^{-1}$)	D_P (nm)
HA	14.6	0.06	2.5
HA-3BN	10.1	0.03	2.0
HA-10BN	9.4	0.02	2.0

inserted in the HA phase. This fact suggests that the reinforcement phase can fill the pores, as well as the blanks between the particles, which decreases the adsorption of N_2 through the test. This can be attributed due to the BN morphology being long sheets.

This fact is a good result for the desired application once the mechanical properties of the material tend to improve with the reduction of pores, since these can act as stress concentrators, resulting in a decrease in the mechanical strength of the material [23].

SEM and TEM

The images obtained through SEM for the BNNS, HA and their composites are in Fig. 6 and the images obtained by TEM are in Fig. 7. It was possible to note that the h-BN sheets are deposited on top of each other. This fact occurs due to van der Waals interactions between the layers and electrostatic interactions due to the electronegativity difference between the B and N atoms [36]. Each sheet has around 14 nm of thickness and hundreds of nanometers wide.

It is notable that the particles of the samples of HA present an oval morphology which agrees with other works using the same sintering temperature [37, 38].

The nanocomposites HA-3BN and HA-10BN present the same morphology, indicating that there was no BNNS interference in the nanostructural characteristics of the samples. However, according to the particle size distribution, in Fig. 6, it is suggested that there was interference in the growth of the particles when BNNS was added. HA particles have an average size of 110 nm, while those of 3% and 10% nanocomposites have 89 nm and 40 nm, respectively.

All samples were synthesized using the hydrothermal method. In this method, after nucleation, there is the growth phase, which is controlled by the saturation of the medium. In nanocomposites, this saturation was unbalanced when adding the reinforcement phase to the precursor solution [4], so this fact may have prevented the proper growth of the particles, as happened with the

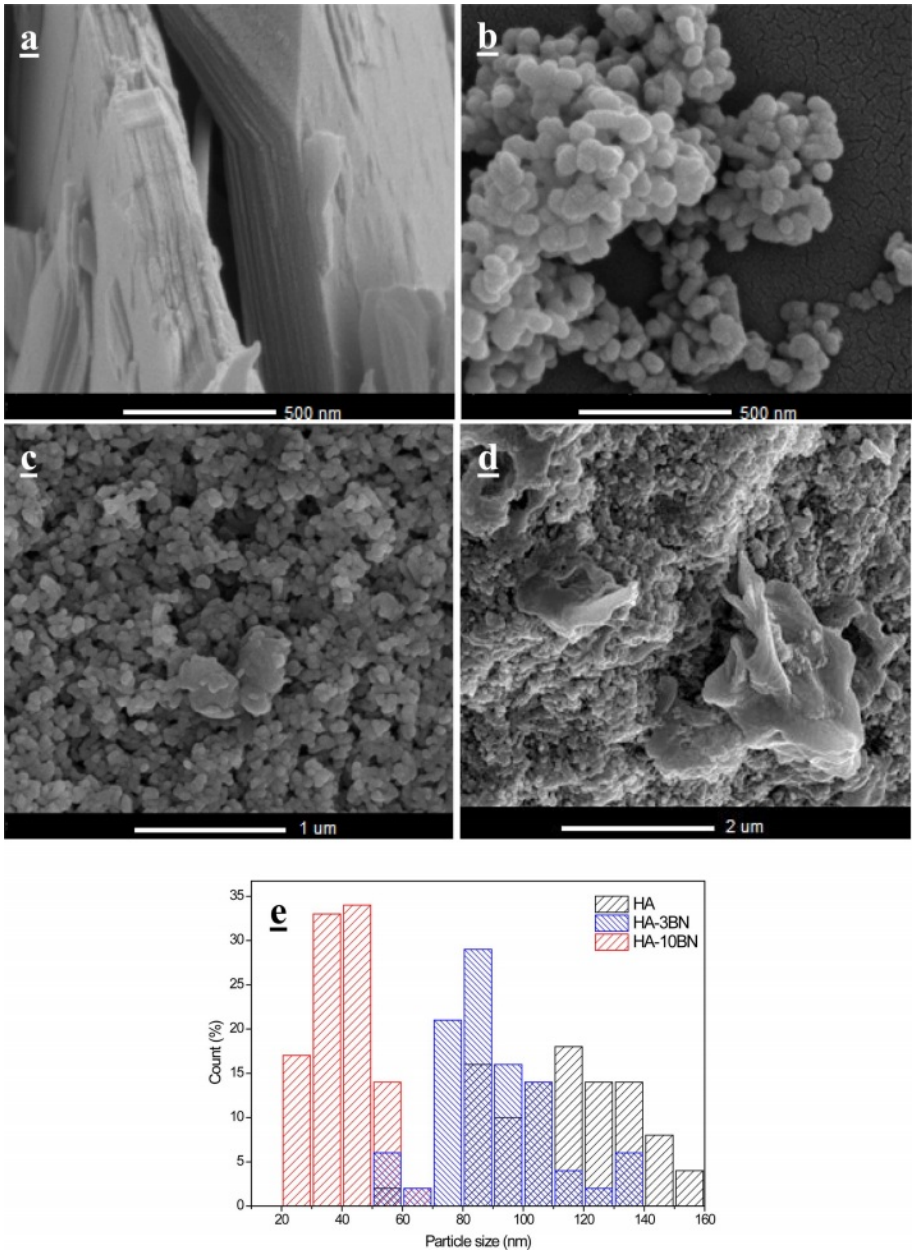

Fig. 6. SEM image of a) BNNS, b) HA, c) HA-3BN, d) HA-10BN and e) particle size distribution of HA and nanocomposites.

HA sample. It is known that HA particles with sizes smaller than 100 nm are perceived to be helpful and potentially ideal for orthopedic applications. Decreasing the size of the particles leads to superior functional properties of the replaced tissue which improves the contact reaction and the stability at the artificial/natural bone interface. It was reported that nano-HA particles with diameters of ~20 nm have shown the best effect on the promotion of cell growth and inhibition of cell apoptosis on human osteoblast-like MG-63 cells in vitro as compared with ~80 nm [39]. Thus, reducing the particle size can be beneficial to the system.

Mechanical properties

The mechanical tests results of HA and composites are presented in Table 2. The nanocomposites showed excellent behavior in the Vickers microhardness test (H_V). With the addition of 3% of the BNNS phase in the system, a 90% increase in the value of H_V can be observed. This increase is already very significant for this system. However, when using 10% of the reinforcement phase, this value changes substantially, going from 0.38 to 2.74 GPa - a 620% increase in the hardness of this proposed system. This fact suggests a strong influence of BNNS on the hardness of the material since BNNS has 48 GPa of hardness [40]. Lahiri et al. report in their research a 100% increase in hardness when they add 4% of BNNT to HA [10]. Similarly, Prajatelistia et al. noticed a 20% increase in hardness by adding 4% h-BN to HA [41]. Despite that,

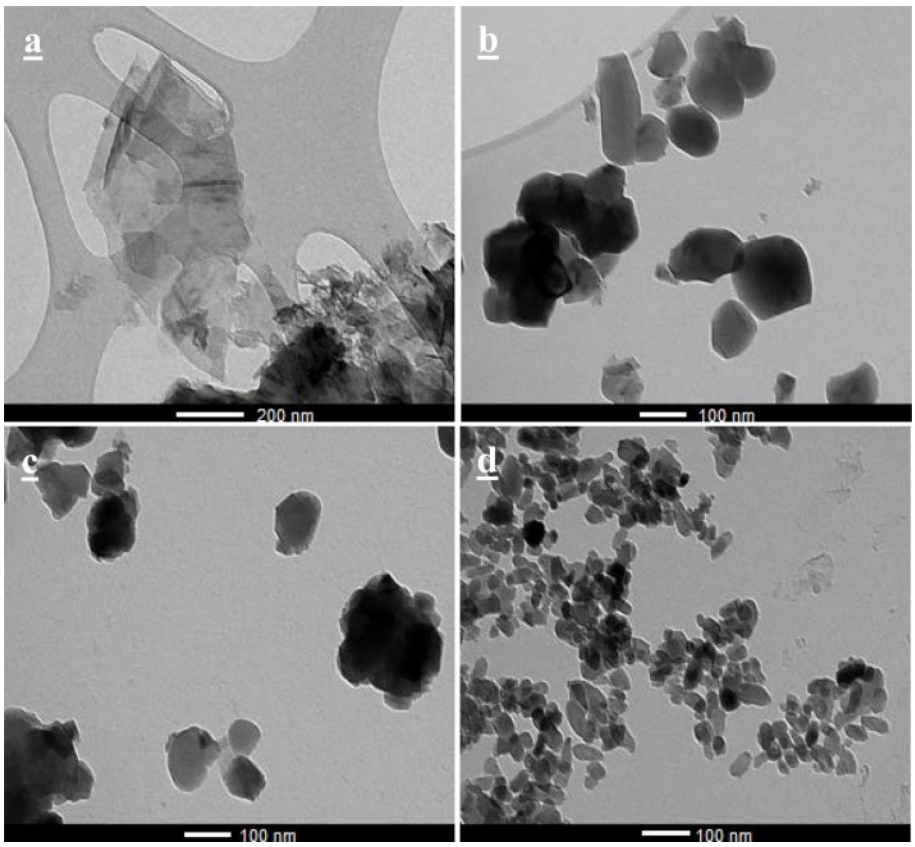

Fig. 7. TEM image of a) BNNS sample, b) HA, c) HA-3BN and d) HA-10BN nanocomposite.

Table 2. Mechanical properties of nanocomposites.

Nanocomposite specimens	H_V (GPa)	Fracture Toughness (MPa)	E (GPa)
HA	0.38 ± 0.09	0.60 ± 0.05	39 ± 5
HA-3BN	0.72 ± 0.05	0.96 ± 0.05	43 ± 4
HA-10BN	2.74 ± 0.39	2.46 ± 0.23	95 ± 9

Aguirre et al., reported a 14% decrease in hardness by adding 2% of BNNP to HA [23]. Wang et al., also noticed a decrease in hardness, of approximately 11%, adding 0.75% h-BN to HA [24].

Vickers indentation method has been used to determine the fracture toughness of the nanocomposite using the radial crack measurement method. Indent on 3% and 10% nanocomposites show significantly smaller impressions with shorter radial cracks as compared to the HA sample. It is noted an improvement of 60% when 3% of BNNS is added to the matrix and 310% when 10% of BNNS is added to the matrix. It is suggested that BNNS acts as a bridging crack for the radial crack, making it shorter. Once the crack is propagating in the matrix and finds BNNS, it needs more energy to overcome this obstacle. Compared with other results of HA-BN nanocomposites [10, 11, 23, 24] the present study shows a more effective improvement in the fracture toughness. This result is promising for the potential use of BNNS-HA nanocomposite in major load-bearing situations and is close to that found for cortical bone, which is about 2 MPa [9].

Measurement of the elastic modulus (E) is performed on the polished cross section of the sintered pellets through the nanoindentation test. Since nanoindentation provides localized mechanical properties, more than 30 indents were made at randomly chosen regions in each sample. The representative load vs. displacement curves for HA, HA-3BN and HA-10BN are shown in Fig. 8. Low indentation depth indicates higher hardness for nanocomposites, once compared to HA sample, which agrees with the Vickers microhardness test result.

Elastic modulus values, calculated from the unloading part of the load-displacement curves, show a higher value for HA-BNNS nanocomposites when compared to HA, as can be seen in Table 6. BNNS reinforcement increases the E of the HA matrix by 10% when 3% of BNNS was added and 143% when 10% of BNNS was added. The improvement in elastic modulus with BNNS addition can be attributed to the factor of BNNS has a higher elastic modulus (~800 GPa) when compared to HA [20]. During the application of stress, the load is transferred from the HA matrix to BNNS. As a result, the resultant strain in nanocomposites is lower than HA. Reduction in the elastic strain causes an increase

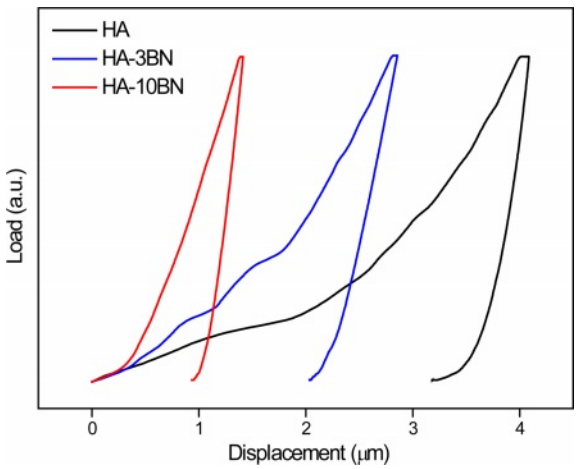

Fig. 8. Load X Displacement plot for nanocomposites obtained by nanoindentation test.

in E for the nanocomposites [10].

Drug loading and in vitro releasing

Through the elemental analysis of C, shown in Table 3, it was possible to estimate the amount of ciprofloxacin (CP) incorporated into the system. CP, of molecular formula $C_{17}H_{18}FN_3O_3$, presented an amount of 62% of carbon, which generated the appearance of this element in the samples since they do not have C in their composition. Thus, the elemental analysis of carbon revealed an increase in the percentage of C in the drug-incorporated samples.

These results agree with those found through the TG test, as shown in Table 3 and Fig. 9-a. The samples did not show a loss of mass in this temperature range, but when incorporating the drug, which degrades between 400-600 ºC, there is an evident loss of mass. Thus, through this mass loss, the percentage of C, present in the samples, is estimated.

Table 3. Elemental analysis results, the amount of ciprofloxacin in the sample calculated through carbon content found and the TG mass lost for incorporated samples.

Samples	C (%)	Amount of Ciprofloxacin in the sample	TG mass lost (%) 130ºC-600ºC
HA + CP	8.9 ± 0.3	14%	15% ± 1
HA-3BN + CP	13.3 ± 0.3	21%	20% ± 1
HA-10BN+ CP	24.9 ± 0.3	40%	41% ± 1
CP	62	100%	-

The drug loading efficiency of hydroxyapatite was examined and according to Table 4, the influence of the addition of the BNNS phase on the drug incorporation rate is evident. This can be explained due to interactions of the reinforcement phase with the ciprofloxacin molecule (Fig. 9-b), which presents both a positive charge contribution, through the protonated piperazine

Table 4. Ciprofloxacin incorporation and release rate in samples.

Sample	Ciprofloxacin incorporation (%)	Ciprofloxacin released (%)
HA	29	61
HA-3BN	41	64
HA-10BN	81	67

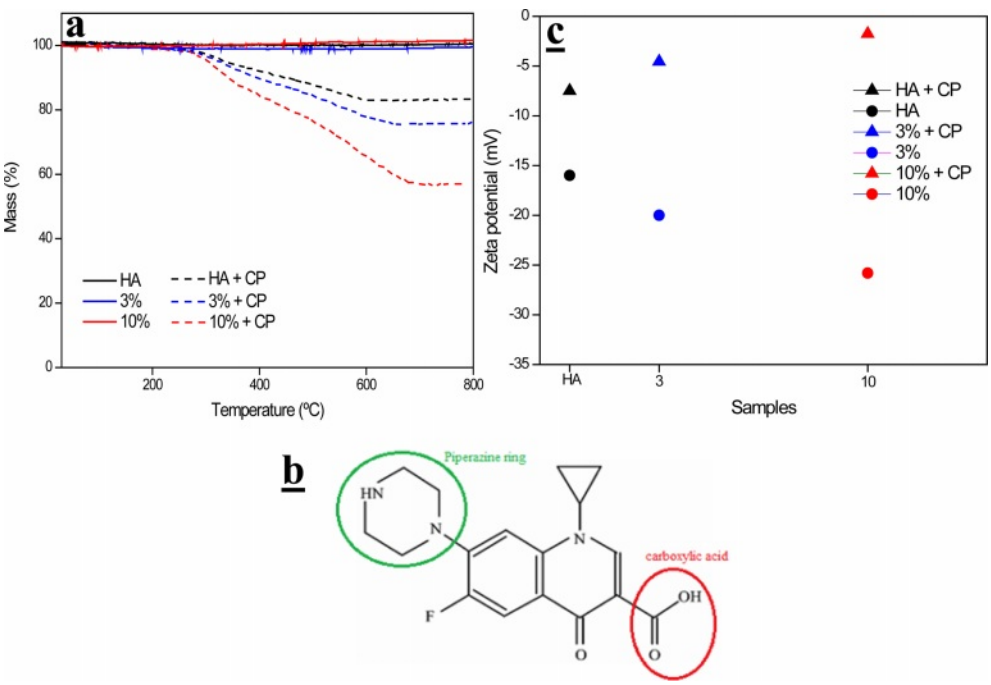

Fig. 9. a) TG analysis of HA and composites, b) CP molecule and c) Zeta Potential of samples before and after CP incorporation.

ring, and a negative charge contribution, through the dissociated carboxylic acid. Thus, the hydroxyls, from the BN purification process, can perform hydrogen interactions with the groups present in the drug molecule. In fact, changes in surface charge can be observed by analyzing the Zeta potential of the samples. It can be seen, through Fig. 9-c, that all samples increased their surface charge values, that is, decreased their negative modules, when incorporating the drug. This may also be evidence that interactions occur between the drug and the samples.

In the HA sample, the drug can be incorporated into the structure of the HA molecule, in its pores, and adsorbed on its surface. In addition, hydroxyl, present in HA, interacts with the groups present in the drug molecule, being also responsible for part of the incorporation of ciprofloxacin in HA.

The release of ciprofloxacin from HA and composites are reported in Fig. 10-a. The drug release is high during the initial time and then it reduces and becomes constant.

For the kinetic studies of the release tests, the data obtained were adjusted to the Korsmeyer-Peppas equation [42, 43]:

$$\frac{M_t}{M_0} = kt^n$$

Where the variable Mt indicates the amount of drug released by the material at time t while Mo represents the amount of drug initially incorporated into the material. The term n indicates the variation of diffusion rate as a function of the release time and k represents a proportionality factor.

The cumulative release against time to the power of 0.50 is presented in Fig. 10b-d. In this representation, the linearity of data is representative of a Fickian diffusion regime as shown in Table 5.

Analyzing region 1 of the samples, two different slopes were found, and good linearity was verified with the Fickian regime. The HA sample presented a higher K value for region A, indicating that the CP release is faster when compared to region B. This fact could be associated with the desorption of ciprofloxacin molecules

Table 5. Results of Fickian model with regard to K and R^2.

Sample	Region	n	K	R^2
HA	1A	0.5	36.1	0.99
	1B	0.5	4.8	0.99
3%	1A	0.5	18.2	0.99
	1B	0.5	3.8	0.99
10%	1A	0.5	15.8	0.99
	1B	0.5	3.1	0.99

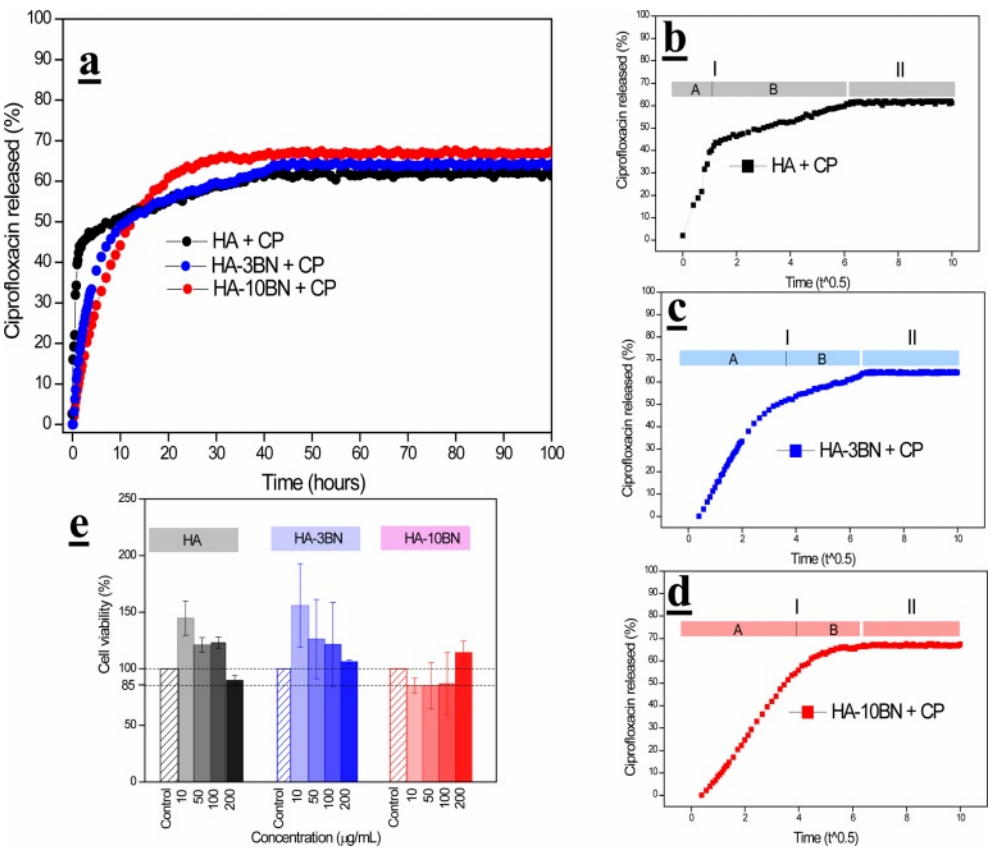

Fig. 10. a) In vitro release of ciprofloxacin, b) CP release against time to the power 0.5 for HA, c) CP release against time to the power 0.5 for HA-3BN, d) CP release against time to the power 0.5 for HA-10BN and e) MTT tests results for HA and composites.

that are located on the surface of the particles. These CP particles do not strongly interact with the hydroxyapatite nanoparticles. In the HA sample, the diameter and volume of pores, as well as the surface area are larger, when compared to composites, thus, desorption is faster. Gradually, with the insertion of the reinforcement phase, the diameters and volume of pores decrease, making it difficult for the desorption of the CP. There is then a decrease in K, indicating that this release occurs more slowly in the 10% composite.

In the B regions of all samples, the value of K is lower, indicating the desorption through micropores present in the samples [44]. On the other hand, region 2 of HA and composites indicates the release of CP, very slowly, through the dissociation of the H bonds between the CP molecule and OH groups of the samples.

Devanan et al., 2011 describe a system composed of HA and Zn with the incorporation of ciprofloxacin, and similar behavior was found [45]. Jariya et al., 2021 synthesized an HA/chitosan scaffold with the incorporation of the same antibiotic and the result was also similar, with a fast and efficient drug release in the first 24 h [46].

The results obtained in this work result is valid, considering that the minimum inhibitory concentration of ciprofloxacin is low (0.25-2 μg/mL) and all samples presented amounts released within this concentration range [45].

Such release profile could provide rapid delivery of the drug giving antibacterial effects at the infected site aiding healing and avoiding toxic and adverse systemic effects.

MTT

Through Fig. 10-e it is possible to observe the graph of cell viability obtained through the MTT test for the biocompatibility assay of HA, 3% and 10% samples in cells of human fibroblasts. It is known that for the use of nanomaterials in biological systems, they must not be toxic to cells. In general, there is an increase in the cell population in relation to concerning the control group. This result is an indication that all samples are biocompatible.

It is noted that with the addition of the reinforcement phase, this cell viability is maintained, for the 3% composites, and decreases for the 10% composites, which may be an indication of the influence of BNNS on the biocompatibility of the material.

Lahiri et al., noticed similar behavior when evaluating the biocompatibility of the HA/BNNT system [10]. Research was carried out by Ciofani evaluating the cytotoxicity of BN nanostructures and it was indicated that the cell viability decreased with respect to controls only at concentrations superior to 50 μg mL^{-1}, and cell proliferation was nonimpacted. That fact proved that even at concentrations as high as 200 μg mL^{-1}, boron nitride particles would still be biocompatible [47]. Furthermore, non-significant statistical tests in relation to control, concentrations and materials were found. That way it is safe to say that even for the lowest values found, the material can still be considered biocompatible, with about approximately 85% of its cell viability.

Conclusion

The synthesis of HA, BNNS, and nanocomposites was effective since the results obtained from XRD, FTIR, SEM, and TEM characterized the material obtained. The increase in hardness, fracture resistance, and elastic modulus of the material is evident when the reinforcement phase is added, thus indicating that the material can expand its application to areas that require heavier efforts. In addition, the cytotoxicity assay, MTT, revealed that HA and its composites have excellent cell viability, and its use as a biomaterial is indicated. The incorporation of the antibiotic ciprofloxacin was effective and greater for the composites when compared to HA, and the interactions between the functional groups present in the drug and the hydroxyl of the BNNS were responsible for this effect. The release of CP also accomplished the expectations of the work, as the material showed a fast initial release, followed by a slow and steady release. In this way, the potential for bifunctionality of the bioceramic material was reached.

Acknowledgments

This research was supported by the Fundação de Amparo à Pesquisa do Estado de Minas Gerais—FAPEMIG, Conselho Nacional de Desenvolvimento Científico e Tecnológico—CNPq and Coordenação de Aperfeiçoamento de Pessoal de Nível Superior—CAPES. The authors thank the Microscopy Center of the Federal University of Minas Gerais, Belo Horizonte, Brazil for the analyses involving electron microscopy.

References

1. H. Qu, H. Fu, Z. Han, and Y. Sun, RSC Adv. 9[45] (2019) 26252-26262.
2. T.T. Roberts and A.J. Rosenbaum, Organogenesis 8[4] (2012) 114-124.
3. A. Farzadi, M. Solati-Hashjin, F. Bakhshi, and A. Aminian, Ceram. Int. 37[1] (2011) 65-71.
4. G. Singh, R.P. Singh, and S.S. Jolly, J. Sol-Gel Sci. Technol. 94[3] (2020) 505-530.
5. S. Bose and S. Tarafder, Acta Biomaterialia 8[4] (2012) 1401-1421.
6. S. Ramesh et al., J. Ceram. Process. Res. 16[6] (2015) 683-689.
7. M.H. Nazarpak, M. Solati-Hashjin, and F. Moztarzadeh, J. Ceram. Process. Res. 10[1] (2009) 54-57.
8. G. Goller, H. Demirkiran, F.N. Oktar, and E. Demirkesen,

Ceram. Int. 29[6] (2003) 721-724.
9. A.A. White, S.M. Best, and I.A. Kinloch, Int. J. Appl. Ceram. Technol. 4[1] (2007) 1-13.
10. D. Lahiri, V. Singh, A.P. Benaduce, S. Seal, L. Kos, and A. Agarwal, J. Mech. Behav. Biomed. Mater. 4[1] (2011) 44-56.
11. T. Lei, L. Wang, C. Ouyang, N.F. Li, and L.S. Zhou, Int. J. Appl. Ceram. Technol. 8[3] (2011) 532-539.
12. X.Y. Lu et al., Appl. Surf. Sci. 262 (2012) 110-113.
13. S. Saber-Samandari, H. Yekta, S. Ahmadi, and K. Alamara, Int. J. Biol. Macromol. 106 (2018) 481-488.
14. J. Nie, J. Zhou, X. Huang, L. Wang, G. Liu, and J. Cheng, Ceram. Int. 45[11] (2019) 13647-13655.
15. C.R.D. Ferreira et al., Ceram. Int. 48[9] (2022) 12376-12386.
16. A.A. Al-Allaq, J.S. Kashan, M.T. El-Wakad, and A.M. Soliman, J. Ceram. Process. Res. 22[4] (2021) 446-454.
17. C. Zhi, Y. Bando, C. Tang, and D. Golberg, in Materials Science and Engineering R: Reports, Nov., 70[3-6] (2010) 92-111.
18. G. Ciofani and V. Mattoli in "Boron Nitride Nanotubes in Nanomedicine" (Elsevier, 2016) p. 1-9.
19. M.G. Rasul, A. Kiziltas, B. Arfaei, and R. Shahbazian-Yassar, 2D Mater. Appl. 5[1] (2021).
20. L. Boldrin, F. Scarpa, R. Chowdhury, and S. Adhikari, Nanotechnology 22[50] (2011).
21. A. Merlo, V.R.S.S. Mokkapati, S. Pandit, and I. Mijakovic, Biomater. Sci. 6[9] (2018) 2298-2311.
22. C. Gao, P. Feng, S. Peng, and C. Shuai, Acta Biomater. 61 (2017) 1-20.
23. T.G. Aguirre, C.L. Cramer, V.P. Torres, T.J. Hammann, T.B. Holland, and K. Ma, J. Mech. Behav. Biomed. Mater. 93[October 2018] (2019) 105-117.
24. C. Wang et al., J. Mater. Sci. 55[29] (2020) 14501-14515.
25. G.R. Anstis, P. Chantikul, B.R. Lawn, and D.B. Marshall, J. Am. Ceram. Soc. 64[9] (1981) 533-538..
26. C.H. Lee, M. Xie, V. Kayastha, J. Wang, and Y.K. Yap, Chem. Mater. 22[5] (2010) 1782-1787.
27. S. Koutsopoulos, J. Biomed. Mater. Res. 62[4] (2002) 600-612.
28. M.F. Cipreste et al., Mater. Chem. Phys. 254 (2020) 123265.
29. R.C.R. dos Apostolos, M.F. Cipreste, R.G. de Sousa, and E.M.B. de Sousa, J. Nanoparticle Res. 22[12] (2020).
30. L. Jun, X. Shuping, and G. Shiyang, Spectrochim. Acta Part A Mol. Spectrosc. 51[4] (1995) 519-532.
31. P.E. Wang and T.K. Chaki, J. Mater. Sci. Mater. Med. 4[2] (1993) 150-158.
32. W. da Silva, H. Ribeiro, T. Ferreira, L. Ladeira, and E. Sousa, Phys. E Low-Dimensional Syst. Nanostructures, 89 (2017) 177-182.
33. T.H. Ferreira, P.R.O. Silva, R.G. Santos, and E.M.B. Sousa, J. Biomater. Nanobiotechnol. 02[04] (2011) 426-434.
34. T.H. Ferreira et al., J. Pharm. Investig. 50[5] (2020) 469-480.
35. K.S.W. Sing et al., Internatuional Union Pure Appl. Chem. IUPAC, (1985).
36. W. Luo, Y. Wang, E. Hitz, Y. Lin, B. Yang, and L. Hu, Adv. Funct. Mater. 27[31] (2017) 1-19.
37. F. Scalera, F. Gervaso, K.P. Sanosh, A. Sannino, and A. Licciulli, Ceram. Int. 39[5] (2013) 4839-4846.
38. E. Landi, A. Tampieri, G. Celotti, and S. Sprio, J. Eur. Ceram. Soc. 20[14-15] (2000) 2377-2387.
39. Z. Shi, X. Huang, Y. Cai, R. Tang, and D. Yang, Acta Biomater. 5[1] (2009) 338-345.
40. D. Lee et al., Small 9[15] (2013) 2602-2610.
41. E. Prajatelistia et al., J. Ceram. Soc. Japan 121[1412] (2013) 344-347.
42. R.W. Korsmeyer, R. Gurny, E. Doelker, P. Buri, and N.A. Peppas, Int. J. Pharm. 15[1] (1983) 25-35.
43. P.L. Ritger and N.A. Peppas, J. Control. Release 5[1] (1987) 37-42.
44. A.L. Doadrio, E.M.B. Sousa, J.C. Doadrio, J. Pérez Pariente, I. Izquierdo-Barba, and M. Vallet-Regí, J. Control. Release 97[1] (2004) 125-132.
45. G. Devanand Venkatasubbu, S. Ramasamy, V. Ramakrishnan, and J. Kumar, 3 Biotech 1[3] (2011) 173-186.
46. S.A.I. Jariya et al., Mater. Chem. Phys. 272 (2021) 125019.
47. G. Ciofani, S. Danti, D.D. Alessandro, S. Moscato, and A. Menciassi, Biochem. Biophys. Res. Commun. 394[2] (2010) 405-411.